Semiconductor Physics, Quantum Electronics & Optoelectronics, 2011. V. 14, N 1. P. 98-105.

PACS 78.20.Fm, 87.64.-t

Mueller-matrix diagnostics of optical properties inherent to polycrystalline networks of human blood plasma

Yu.A. Ushenko[1], O.I. Olar[2], A.V. Dubolazov[3], V.O. Balanetskaya[3], V.P. Unguryan[4], N.I. Zabolotna[5], B.P. Oleinichenko[6]

[1]*Chernivtsi National University, Department for Correlation Optics, 2, Kotsyubinsky vul., 58012 Chernivtsi, Ukraine, yuriyu@gmail.com*

[2]*Bukovina State Medical University, Department of Biophysics and Medical Informatics, 2, Teatralnaya Sq., 58012 Chernivtsi, Ukraine.*

[3]*Chernivtsi National University, Department for Optics and Spectroscopy, 2, Kotsyubinsky vul., 58012 Chernivtsi, Ukraine.*

[4]*Bukovina State Medical University, Department for Oncology, 2, Teatralnaya ploshchad, 58012 Chernivtsi, Ukraine.*

[5]*Vinnytsa National Technical University, Department for Laser and Optoelectronic Technique, 95, Khmelnitskoye shosse, 21021 Vinnytsa, Ukraine.*

[6]*Medical Center "Medivin", 95, Khmelnitskoye shosse, 21021 Vinnytsa, Ukraine.*

Abstract. This work is aimed at studying the possibilities of Mueller-matrix diagnostics applied to optically anisotropic birefringent polycrystalline networks inherent to amino acids in human blood plasma. Determined here are interrelations between statistical moments of the first to fourth orders as well as fractal dimensionalities that characterize coordinate distributions of blood plasma Mueller-matrix elements and the physiological state of a human organism.

Keywords: polarization, Mueller matrix, optical anisotropy, birefringence, statistical moments, fractal, blood plasma.

Manuscript received 07.10.10; accepted for publication 02.12.10; published online 28.02.11.

1. Introduction

Among the diversity of directions for optical diagnostics of the structure typical for phase-inhomogeneous layers, Mueller-matrix polarimetry of optical anisotropy observed in human biological tissues (BT) is rather developed [1 – 39].

The main result of this diagnostics lies in determination of the set of interrelations between statistical as well as fractal parameters of coordinate distributions for matrix elements and an optical-geometrical structure of BT birefringent component [1 – 6, 9, 11, 12, 14, 38]. It serves as a basis to develop the methods for early diagnostics of pathological changes in skin derma, epithelial and connective tissue of woman reproductive organs etc. [11, 14, 21 – 27, 35, 36].

At the same time, one of the lacks of this optical-medical technology is the traumatic biopsy operation. Therefore, it seems topical to spread Mueller-matrix diagnostics over a wide and accessible circle of biological objects. These are various biological liquids, namely: blood, urine, bile, joint fluid, etc.

Our work is aimed at development of the Mueller matrix method for diagnostics of optically anisotropic structure typical for blood plasma proteins, as it is topical to determine statistical and fractal criteria of transformations in amino acid polycrystalline networks, which are caused by pathological changes in human organism.

2. Mueller-matrix modeling the polarization properties of polycrystalline protein networks in blood plasma

Our analysis of optical properties inherent to polycrystalline protein networks created by blood plasma amino acids is based on the following model [5, 6, 15, 23, 28, 29]:

- blood plasma is considered as a two-component isotropic-anisotropic structure;
- a optically anisotropic component is represented by the protein fraction consisting of optically single-axis birefringent crystals of amino acids albumin and globulin;
- polarization properties of these biological crystals are characterized with the Mueller matrix

$$\{z\}_u = \begin{Vmatrix} 1 & 0 & 0 & 0 \\ 0 & z_{22} & z_{23} & z_{24} \\ 0 & z_{32} & z_{33} & z_{34} \\ 0 & z_{42} & z_{43} & z_{44} \end{Vmatrix}, \quad (1)$$

where

$$(z_{ik})_u = \begin{cases} z_{22} = \cos^2 2\rho + \sin^2 2\rho \cos\delta, \\ z_{23,32} = \cos 2\rho \sin 2\rho (1 - \cos\delta), \\ z_{33} = \sin^2 2\rho + \cos^2 2\rho \cos\delta, \\ z_{34,43} = \pm \cos 2\rho \sin\delta, \\ z_{24,42} = \pm \sin 2\rho \sin\delta, \\ z_{44} = \cos\delta. \end{cases} \quad (2)$$

Here, ρ is the direction of the optical axis; $\delta = 2\pi/\lambda \Delta n d$ – phase shift between orthogonal components of the amplitude, λ - wavelength, d - geometric distance, Δn - index of birefringence;

- Mueller matrix elements R_{ik} for the planar network layer (N) of crystalline amino acids are determined by superposition of partial matrix operators (relation (1))

$$R_{ik} = \sum_{u=1}^{N} (z_{ik})_u , \quad (3)$$

- Mueller matrix of multilayer (n) polycrystalline network is determined with the product of partial matrix operators (relation (3))

$$\{P\} = \{R\}_n \{R\}_{n-1} \ldots \{R\}_2 \{R\}_1 , \quad (4)$$

To simplify (without any losses of fullness) our consideration, let us use the approximation of two-layer polycrystalline protein network

$$\{P\} = \{R\}_2 \{R\}_1 \equiv \{Y\}\{X\}. \quad (5)$$

In a detailed look, the expression (5) can be written as

$$p_{ik} = \begin{cases} p_{22} = y_{22}x_{22} + y_{23}x_{32} + y_{24}x_{42}, \\ p_{23} = y_{22}x_{23} + y_{23}x_{33} + y_{24}x_{43}, \\ p_{32} = y_{32}x_{22} + y_{33}x_{32} + y_{34}x_{42}, \\ p_{33} = y_{32}x_{23} + y_{33}x_{33} + y_{34}x_{43}, \\ p_{34} = y_{32}x_{24} + y_{33}x_{34} + y_{34}x_{44}, \\ p_{43} = y_{42}x_{23} + y_{43}x_{33} + y_{44}x_{43}, \\ p_{24} = y_{22}x_{24} + y_{23}x_{34} + y_{24}x_{44}, \\ p_{42} = y_{42}x_{22} + y_{43}x_{32} + y_{44}x_{42}, \\ p_{44} = y_{42}x_{24} + y_{43}x_{34} + y_{44}x_{44}. \end{cases} \quad (6)$$

Our analysis of relations (1), (2), (5) and (6) shows that the exact solution of the inverse problem – revealing the changes in the structure of polycrystalline protein networks in separate layers by using available information on matrix elements p_{ik}, - is incorrect from the mathematical viewpoint and ambiguous from the physical one.

Thus, it seems topical to use the statistical and fractal approaches to the analysis of distributions inherent to Mueller matrix elements in optically anisotropic polycrystalline protein component of blood plasma.

3. Statistical and fractal analyses of Mueller-matrix images for networks of biological crystals

Coordinate distributions of Mueller matrix elements p_{ik} in blood plasma were estimated within the frameworks of statistical and fractal approaches.

The statistical moments of the first to fourth orders that characterize the $p_{ik}(x,y)$ distributions were calculated using the following relations [5, 8]

$$M_1 = \frac{1}{Q}\sum_{j=1}^{N} |p_{ik}|_j ; \; M_2 = \sqrt{\frac{1}{Q}\sum_{j=1}^{N} (p_{ik})_j^{\,2}};$$

$$M_3 = \frac{1}{M_2^{\,3}} \frac{1}{Q} \sum_{j=1}^{N} (p_{ik})_j^3 ; \; M_4 = \frac{1}{M_2^{\,2}} \frac{1}{Q} \sum_{j=1}^{N} (p_{ik})_j^{\,4} , \quad (7)$$

where Q! is the number of pixels in CCD camera.

The fractal analysis of $p_{ik}(x,y)$ distributions was made by finding the logarithmic dependences $\log J(p_{ik}) - \log(d^{-1})$ for the power spectra $J(p_{ik})$ [5, 15]

$$J(p_{ik}) = \int_{-\infty}^{+\infty} p_{ik} \cos 2\pi\nu d\nu , \quad (8)$$

where $\nu = d^{-1}$ are spatial frequencies determined by the range of changing the sizes d of structural elements in the polycrystalline network.

The dependences $\log J(p_{ik}) - \log(d^{-1})$ were approximated using the least-squares method to the curves $\Phi(\eta)$, straight parts of which allow determining the slope angles η and respective fractal dimensionalities [5, 15]

$$D = 3 - tg\eta . \quad (9)$$

Classification of coordinate distributions $p_{ik}(x,y)$ was performed in accord with the following criteria:

- $p_{ik}(x,y)$ are fractal or self-similar, if η = const within the limits of 2 or 3 decades for changing the geometric sizes d;
- $p_{ik}(x,y)$ are multifractal when several constant slope angles $\eta_{j=1;2;\ldots} = \text{const}$ are available:
- $p_{ik}(x,y)$ are statistical or random, if $\eta \neq \text{const}$ over all the interval for changing d.

4. Scheme and method of measurements

Shown in Fig. 1 is the traditional optical scheme of the polarimeter used for measuring the coordinate distributions of Mueller matrix elements or Mueller-matrix images (MMI) [5].

Illumination of blood plasma samples was made with a parallel ($\Delta \Subset 2\times10^3\,\mu m$) weakly intense (W = 5.0 mW) beam of He-Ne laser (λ = 0.6328 μm). The polarization illuminator consists of quarter-wave plates 3, 5 and the polarizer 4, which provides formation of the laser beam with an arbitrary azimuth and ellipticity of polarization.

The studied human blood plasma sample was sequentially probed with the laser beam possessing the following types of polarization: linear with the azimuths 0°, 90°, +45° and right circular (⊗). Using the micro-objective 7, the polarization images were projected onto the plane of the sensitive area ($m\times n = 800\times600$ pixels) of CCD camera 10. The analysis of images of human blood plasma was made using the analyzer 9 and quarter-wave plate 8.

Our calculation of Mueller matrix elements for the studied samples was performed in accord with the following algorithm [5]

$$
\begin{aligned}
&p_{11}=0{,}5(S_1^0+S_1^{90}); && p_{21}=0{,}5(S_2^0+S_2^{90});\\
&p_{12}=0{,}5(S_1^0-S_1^{90}); && p_{22}=0{,}5(S_2^0-S_2^{90});\\
&p_{13}=S_1^{45}-p_{11}; && p_{23}=S_2^{45}-p_{21};\\
&p_{14}=S_1^{\otimes}-p_{11}; && p_{24}=S_2^{\otimes}-p_{21};\\
&p_{31}=0{,}5(S_3^0+S_3^{90}); && p_{41}=0{,}5(S_4^0+S_4^{90});\\
&p_{32}=0{,}5(S_3^0-S_3^{90}); && p_{42}=0{,}5(S_4^0-S_4^{90});\\
&p_{33}=S_3^{45}-p_{31}; && p_{43}=S_4^{45}-p_{41};\\
&p_{34}=S_3^{\otimes}-p_{31}; && p_{44}=S_4^{\otimes}-p_{41}.
\end{aligned}
\qquad (10)
$$

Here, $S_{j=1;2;3;4}^{0;45;90;\oplus}$ are the Stokes vector parameters.

5. Brief characterization of the investigated objects

As objects of investigation, we chose the samples of blood plasma for two groups of patients: healthy woman and that with cancer of mammary gland (Figs 1c and 1d). The respective polycrystalline networks for blood plasma amino acids are illustrated with a set of laser images obtained in co-axial ($\Theta = 0^0$) and crossed ($\Theta = 90^0$) transmission planes of the polarizer 4 and analyzer 9 (Fig. 1).

Our comparative analysis of these laser images found out different coordinate structures for albumin and globulin networks. In the optically anisotropic component of healthy woman blood plasma, one can observe albumin crystals spatially-ordered along several directions (Figs 1a and 1b). While blood plasma of the patient with the oncologic process contains mainly globulin crystals disordered as to directions of optical axes (Figs 1c and 1d).

6. Diagnostic possibilities for statistical and fractal analyses of Mueller-matrix images obtained for human blood plasma

The subject of our statistical and fractal analyses was three types of Mueller-matrix images $p_{ik}(m\times n)$ for human blood plasma.

The first one is the coordinate distributions of diagonal elements in the Mueller matrix $p_{22;33}(m\times n)$, which characterize the degree of transformation of the laser wave polarization azimuth by amino acid crystals, optical axes of which are oriented along two mutually orthogonal directions $\rho = 0^0 \leftrightarrow 90^0$ ($p_{22}(m\times n)$) and

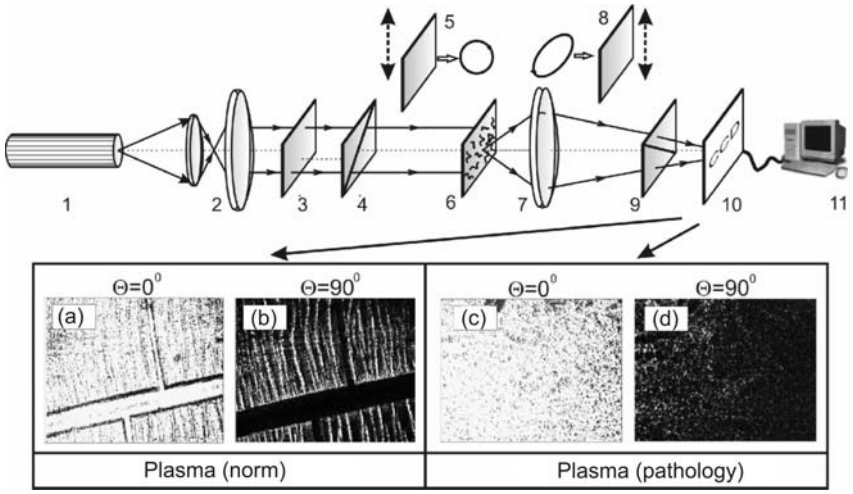

Fig. 1. Optical scheme of the polarimeter: 1 – He-Ne laser; 2 – collimator; 3 – stationary quarter-wave plate; 5, 8 – mechanically movable quarter-wave plates; 4, 9 – polarizer and analyzer, respectively; 6 – studied object; 7 – micro-objective; 10 – CCD camera; 11 – personal computer. See explanation in the text.

$\rho = 45^0 \leftrightarrow 135^0$ ($p_{33}(m \times n)$), respectively. In this sense, these matrix elements will be named as the "orientational" ones.

The second type is coordinate distributions for the diagonal matrix element $p_{44}(m \times n)$, the value of which is determined by phase shifts between orthogonal components for the laser wave amplitude that artise as a consequence of birefruingence caused by crystalline amino acids. In this sense, this element of the Mueller matrix will be named as "phase" one.

The third type is coordinate distributions of off-diagonal elements in the Mueller matrix $p_{23;24;34}(m \times n)$, which characterize mechanisms of mutual transformations of linear polarization into a elliptic one, and vice versa. These matrix elements will be named as the "orientational-phase" ones.

Shown in Fig. 2 are the results of investigations of the following MMI structures observed for blood plasma of the healthy patient: coordinate ($p_{ik}(m \times n)$, left column), statistical (histograms $h(p_{ik})$ and statistical moments of the first and fourth orders $M_{j=1;2;3;4}$, central column) as well as fractal (logarithmic dependences $\log J(p_{ik}) - \log(d^{-1})$, right column).

Our analysis of the obtained data enabled us to reveal:

"Orientational" matrix elements $p_{22;33}(m \times n)$

Histograms $h(p_{22})$ and $h(p_{33})$ are characterized with pronounced main extremes. Formation of these extremes may be related with superposition of matrix elements $p_{22;33}(m \times n)$ (relations (3)), values of which are determined by albumin crystals ordered relatively two or three separated directions of optical axes (relations (2), Figs 1a and 1b).

The most pronounced differentiation of the coordinate distributions for matrix elements $p_{22}(m \times n)$ and $p_{33}(m \times n)$ of the polycrystalline network in blood plasma can be realized using the statistical moments of the third and fourth orders. Differences between the values $M_3(p_{22;33})$ and $M_4(p_{22;33})$ in these distributions can reach 4 and 2.5 times, respectively (Fig. 2, central column).

Our analysis of the dependences $\log J(p_{22}) - \log(d^{-1})$; $\log J(p_{33}) - \log(d^{-1})$ allowed us to reveal stability in the values of slope angles η within the range of changes in geometric sizes d of amino acid crystals from 50 up to 1000 μm (Fig. 2, right column). This result is indicative of the fractal structure inherent to the distributions of $Z_{22;33}(m \times n)$, which can be related with an order of optical axis directions ρ for albumin crystals. By contrast, disorder in globulin crystal orientations within the range of lower geometric sizes ($d = 2 \ldots 50$ μm) causes randomness in coordinate distributions of $p_{22;33}(m \times n)$. Quantitatively, this fact is expressed through the absence of any stable slope angle for the dependences $\log J(p_{22}) - \log d^{-1}$; $\log J(p_{33}) - \log d^{-1}$.

*"**Phase" matrix elements*** $p_{44}(m \times n)$

The histogram $h(p_{44})$ for the distribution of values inherent to the "phase" matrix element for blood plasma of healthy woman is characterized by a wide range of changes in p_{44} values caused by variations of geometric sizes ($d = 1 \ldots 1000$ μm) of albumin and globulin crystals (relation (2)).

The coordinate distribution of $p_{44}(m \times n)$ is multifractal, since the curves $\Phi(\eta)$ approximating the logarithmic dependences $\log J(Z_{44}) - \log d^{-1}$ are polygonal lines with several slope angles η (Fig. 2, right column).

The found multifractality of the distribution corresponding to the "phase" matrix element $p_{44}(m \times n)$ of blood plasma is apparently caused by multiple changes ($\delta = \delta + 2k\pi, k = 0;1;2;\ldots$) in phase shifts δ, which is related with different scales of geometric sizes inherent to albumin (50…1000 μm) and globulin (1…50 μm) crystals.

"Orientational -phase" matrix elements $p_{23;24;34}(m \times n)$

The histograms $h(p_{23})$, $h(p_{24})$ and $h(p_{34})$ for the distributions $p_{23;24;34}(m \times n)$ are practically "equiprobable". Here, we do not take into account the main extreme $h(p_{23;24;34}) \to 0$, formation of which is caused by the influence of optically isotropic component in blood plasma.

The wide range of changes in local extremes $h(p_{23;24;34}) \neq 0$ can be related with a simultaneous influence of both optical axis orientation ρ and phase shift δ (relations (2) and (3)) for local crystals in albumin-globulin blood plasma network on formation of the value of "orientational-phase" matrix elements.

It was ascertained that differentiation of optical properties inherent to these networks can be efficiently performed using determination of the fourth order statistical moments for $p_{23;24;34}(m \times n)$ elements of MMI, because differences between M_4 values reach 3 times.

Our analysis of the power spectra $J(p_{23;24;34})$ found multifractality of distributions for matrix elements $p_{23;24;34}(m \times n)$ corresponding to healthy woman blood plasma. It was ascertained that $p_{23;24;34}(m \times n)$ elements

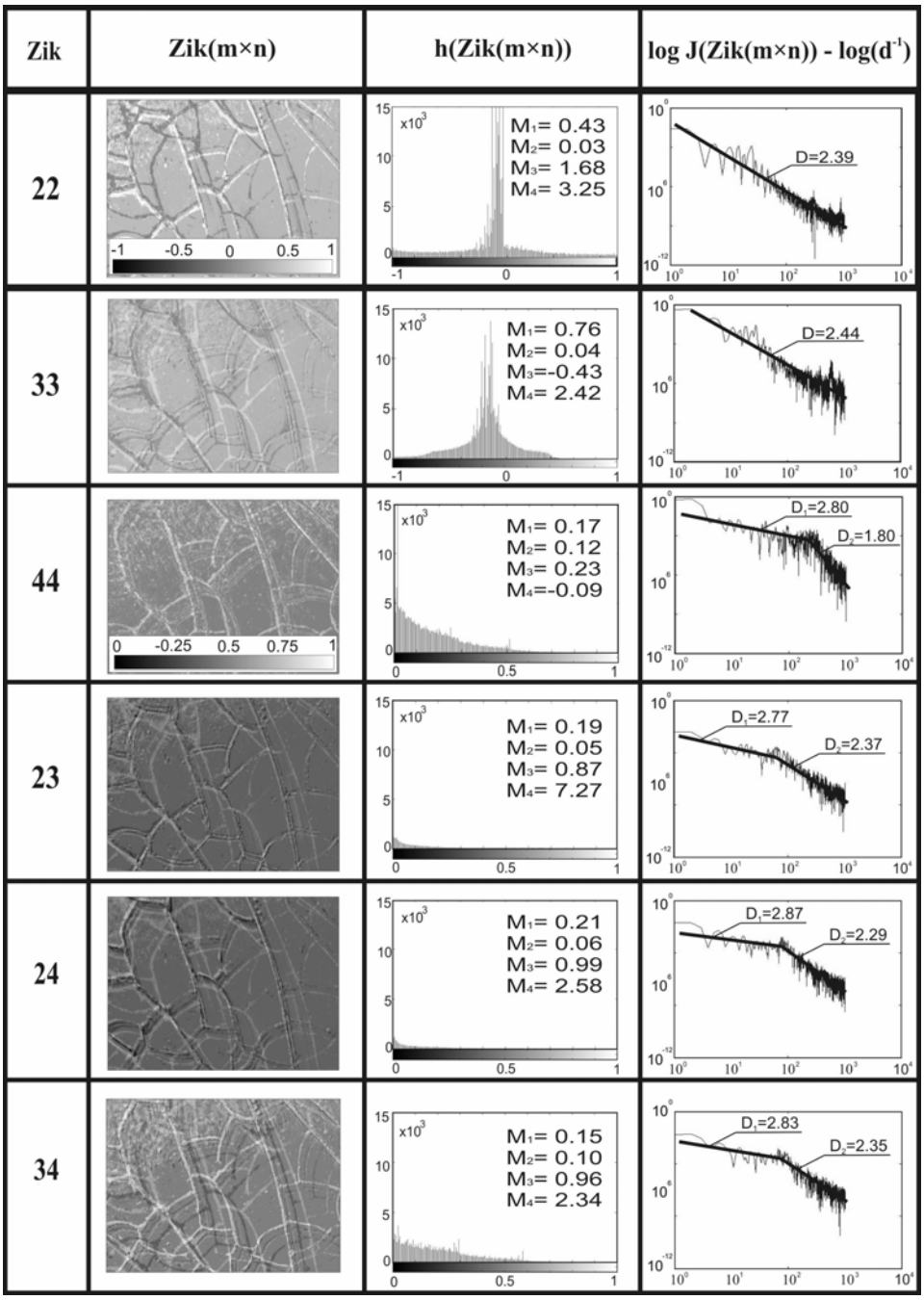

Fig. 2. Statistical and fractal structure of blood plasma MMI for a healthy patient.

in MMI are characterized with individual sets of fractal dimensionalities (Fig. 2, right column).

Shown in Fig. 3 is the set of statistical ($h(p_{ik})$; $M_{j=1;2;3;4}$) and fractal ($\log J(p_{ik}) - \log d^{-1}; F_q$) parameters that characterize $p_{ik}(m \times n)$ elements in MMI of polycrystalline networks of amino acids in blood plasma of the patient with mammary gland cancer.

The analysis of MMI for the respective blood plasma samples found essential transformation of histograms $h(p_{ik})$.

The histograms $h(p_{22})$ and $h(p_{33})$ are characterized with redistribution of extremes, which can be related with changes in orientations of optical axes $\rho(m \times n)$ and phase shift values $\delta(m \times n)$ in the albumin-globulin network of blood plasma (Fig. 3, central column). From the biochemical viewpoint, this process is caused by growth of the globulin concentration in

blood plasma. As a result, we deal with disordering the directions of optical axes inherent to globulin crystals and growth of their birefringence. Therefore, the range of changes in values of "orientational" matrix elements $p_{22;33}$ is expanded, and the main extremes $h(p_{22} \to 1)$, $h(p_{33} \to 1)$ are "shifted" (relations (2), (3)).

Changes in birefringence of blood plasma polycrystalline network observed in the samples taken from patients with mammary gland cancer are also pronounced in formation of practically equiprobable distributions of "phase" p_{44} and "orientational-phase" $p_{23;24;34}$ matrix elements.

The analysis of the power spectra $J(p_{ik})$ for pathologically changed blood plasma found the tendency to growth of the amount of fractal dimensionalities for coordinate distributions of "orientational" $p_{22;33}(m \times n)$, "orientational-phase" $p_{23;24;34}(m \times n)$ and "phase" elements $p_{44}(m \times n)$ (Fig. 3, right column).

With the aim to determine the quantitative Mueller-matrix statistical and fractal criteria for differentiation of polycrystalline protein networks of amino acids, we have investigated blood plasma samples taken from two groups of patients, namely: healthy ones (21 persons) and those sick of cancer (19 persons).

Summarized in Table 1 are the statistical moments from the first to fourth orders that characterize coordinate distributions of "orientational" $p_{22;33}$, "orientational-phase" $p_{23;24;34}$ and "phase" p_{44} elements of the Mueller matrix corresponding to blood plasma of both groups.

Our comparative analysis of the values and ranges for changes of statistical parameters M_j found for blood plasma of healthy patients and those sick of cancer enabled us to reveal the following features:

- asymmetry values M_3 for the distributions of "orientational" matrix elements $p_{22;33}(m \times n)$ describing blood plasma of oncologically sick patients decrease by 1.4 to 5 and 1.8 to 7.5 times, respectively;
- excess M_4 for the coordinate distribution of the "phase" element $p_{44}(m \times n)$ corresponding to pathologically changed polycrystalline protein network of amino acids in blood plasma is 20-fold decreased;
- decrease of the values inherent to statistical moments of the third and fourth orders in the coordinate distributions of "orientational-phase" elements in the Mueller matrix $p_{23;24;34}(m \times n)$ reaches 4.3 to 5 and 7 to 20 times, respectively.

p_{ik}	M_j	Norm	Mammary gland cancer
p_{22}	M_1	0.73 ± 0.087	0.72 ± 0.084
	M_2	0.06 ± 0.008	0.07 ± 0.009
	M_3	1.68 ± 0.23	0.31 ± 0.037
	M_4	3.25 ± 0.44	0.47 ± 0.054
p_{33}	M_1	0.76 ± 0.088	0.78 ± 0.084
	M_2	0.04 ± 0.006	0.06 ± 0.008
	M_3	0.43 ± 0.057	0.32 ± 0.039
	M_4	2.42 ± 0.31	1.32 ± 0.18
p_{44}	M_1	0.17 ± 0.022	0.32 ± 0.041
	M_2	0.12 ± 0.018	0.14 ± 0.018
	M_3	0.23 ± 0.033	0.28 ± 0.036
	M_4	2.09 ± 0.27	0.11 ± 0.015
p_{23}	M_1	0.19 ± 0.024	0.16 ± 0.021
	M_2	0.05 ± 0.007	0.03 ± 0.004
	M_3	0.87 ± 0.093	0.16 ± 0.022
	M_4	7.27 ± 0.96	0.35 ± 0.045
p_{24}	M_1	0.21 ± 0.028	0.17 ± 0.024
	M_2	0.06 ± 0.008	0.03 ± 0.005
	M_3	0.99 ± 0.11	0.13 ± 0.017
	M_4	2.58 ± 0.32	2.72 ± 0.33
p_{34}	M_1	0.15 ± 0.019	0.34 ± 0.042
	M_2	0.10 ± 0.012	0.11 ± 0.015
	M_3	0.96 ± 0.099	0.19 ± 0.025
	M_4	2.34 ± 0.28	0.25 ± 0.029

Thus, just the statistical moments of higher orders are the most sensitive to changes in optically isotropic structure of blood plasma.

Table 2 illustrates the values of fractal dimensionalities for $p_{ik}(m \times n)$ elements in MMI of blood plasma in both groups.

The comparative analysis of the obtained data indicates:

- transformation of fractal distributions for "orientational" moments into the multifractal ones;
- 15% to 25% growth of the value and amount of fractal dimensionalities F_q for distributions of "orientational-phase" and "phase" elements.

Thus, it can be contended that biochemical changes in the blood plasma structure are clearly pronounced in changes of statistical and fractal parameters characterizing the set of MMI elements $p_{ik}(m \times n)$ and can be applied as new criteria for diagnostics of human pathological states.

Table 1. Statistical moments for distributions of $p_{ik}(m \times n)$

Table 2. Fractal dimensionalities for distributions of the Mueller matrix elements

Z_{ik}	D_q	Norm	Mammary gland cancer
Z_{22}	D_1	2.12 ± 0.14	2.17 ± 0.18
	D_2	-	1.86 ± 0.15
	D_3	-	2.01 ± 0.21
Z_{33}	D_1	2.09 ± 0.12	2.14 ± 0.14
	D_2	-	1.94 ± 0.13
	D_3	-	2.03 ± 0.19
Z_{44}	D_1	1.98 ± 0.127	2.07 ± 0.21
	D_2	1.76 ± 0.19	1.83 ± 0.17
	D_3	-	2.31 ± 0.24
Z_{23}	D_1	2.07 ± 0.19	2.12 ± 0.18
	D_2	2.18 ± 0.13	2.27 ± 0.19
	D_3	-	1.83 ± 0.13
Z_{34}	D_1	1.83 ± 0.18	1.97 ± 0.21
	D_2	2.05 ± 0.26	2.11 ± 0.14
	D_3	-	1.81 ± 0.16

References

1. de Boer J F and Milner T E 2002 Review of polarization sensitive optical coherence tomography and Stokes vector determination *J. Biomed. Opt.* **7** 359-71
2. de Boer J F, Milner T E and Nelson J S 1998 *Trends in Optics and Photonics (TOPS): Advances in Optical Imaging and Photon Migration* (OSA, Washington, DC).
3. Everett M J, Shoenenberger K, Colston B W and Da Silva L B 1998 Birefringence characterization of biological tissue by use of optical coherence tomography *Opt. Lett.* **23** 228-30.
4. Shuliang J, Wurong Yu, Stoica G and Lihong V 2003 Optical fiber based Mueller optical coherence tomography *Opt. Lett.* **28** 1206-08.
5. Coherent-Domain Optical Methods: Biomedical Diagnostics, Environmental and Material Science / edited by V. V. Tuchin // Laser Polarimetry of Biological Tissue. Principles and Applications / A.G. Ushenko, V.P. Pishak. – *Boston: Kluwer Academic Publishers*, p. 67-93 (2004).
6. A.G. Ushenko, Stokes-correlometry of biotissues // *Laser Physics*. **10**, No.6, p.1-7 (2000).
7. A.G. Ushenko, Yu.Y. Tomka, Laser polarization selection of two-dimensional birefringence images // *Proc. SPIE*. **5972**, p. 59720S (2005).
8. A.G. Ushenko, I.Z. Misevich, V. Istratiy and others. Evolution of statistic moments of 2D-distributions of biological liquid crystals net Mueller matrix elements in the process of their birefringent structure changes // Advances in Optical Technologies, **2010**, Article 1D 423125 (2010).
9. O.V. Dubolazov, A.G. Ushenko, V.T. Bachunsky and others. On the feasibilities of using the wavelet analysis of Mueller matrix images of biological crystals. // Advances in Optical Technologies, **2010**, Article 1D 162832 (2010).
10. A.G. Ushenko, 2D phase tomography of biotissues: II. Polarization visualization and selection of biotissue image two-layer scattering medium // *Proc. SPIE,* **5477**, p. 450-456 (2004).
11. O.V. Angelsky; A.G. Ushenko; Ye.G. Ushenko, 2-D Stokes Polarimetry of Biospeckle Tissues Images in Pre-Clinic Diagnostics of Their Pre-Cancer States // *Journal of Holography and Speckle*, **2**, (1), p. 26-33 (2005).
12. A.G. Ushenko; A.I. Fediv; Yu.F. Marchuk, Correlation and fractal structure of Jones matrices of human bile secret // *Proc. SPIE,* **7368**, 73681Q (2009).
13. A.G. Ushenko, Yu.Ya. Tomka, V.I. Istratiy, Polarization selection of two-dimensional phase-inhomogeneous birefringence images of biotissues // *Proc. SPIE*, **7388**, 73881L (2009).
14. Yu.Ya. Tomka, A.G. Ushenko, Yu. F. Marchuk, The degree of mutual correlation of coordinate distributions of Mueller matrix elements biological tissues and diagnostics of their physiological state // *Proc. SPIE*, **7388,** 73881K (2009).
15. A.G. Ushenko, Laser diagnostics of biofractals // *Quantum Electronic*,.**29** (12), p.1-7 (1999).
16. A.G. Ushenko, The Vector Structure of Laser Biospeckle Fields and Polarization Diagnostics of Collagen Skin Structures // Laser Physics, **10** (5), p.1143-1149 (2000).
17. A.G. Ushenko, 2D phase tomography of biotissues: I. Topological structure value of birefringence // *Proc. SPIE*, **5477**, p.438-449 (2004).
18. A.G. Ushenko, Polarization introscopy of phase-inhomogeneous layers // *Proc SPIE*, **4900**, p.1323-1326 (2002).
19. O.V.Angelsky, A.G. Ushenko, Ye.G. Ushenko, Yu.Ya. Tomka, Polarization singularities of biological tissues images // *J. Biomed. Opt.* **11** (5), p. 054030 (2006).
20. A.G. Ushenko, Laser polarimetry of polarization-phase statistical moments of the objects field of optically anisotropic scattering layers // *Optics and spectroscopy,* **91** (2), p.313-317 (2001).
21. O.V. Angelsky, A.G. Ushenko, Ye.G. Ushenko, Investigation of the correlation structure of biological tissue polarization images during the diagnostics of their oncological changes // *Phys. Med. Biol*. **50**, p.4811-4822 (2005).
22. O.V. Angelsky, V.P. Pishak, A.G. Ushenko, D.N. Burkovets, O.V. Pishak, Polarization-correlation investigation of biotissue multifractal structure and diagnostics of its pathological change // *Proc. SPIE*, **4242**, p.201-209 (2001).
23. O.V. Angelsky, A.G. Ushenko, Ye.G. Ushenko, Complex degree of mutual polarization of

biological tissue coherent images for the diagnostics of their physiological state // *J. Biomed. Opt.* **10** (6), p. 060502 (2005).
24. A.G. Ushenko, S.B. Yermolenko, O.V. Angelsky, V.P. Pishak, O.V. Pishak, Laser polarimetry tomography of biotissue pathological changes // *Proc. SPIE*, **4425**, p.117-123 (2001).
25. A.G. Ushenko, A.I. Fediv, Yu.F. Marchuk, Singular structure of polarization images of bile secret in diagnostics of human physiological state // *Proc. SPIE*, 73681S (2009).
26. S.B. Yermolenko, A.G. Ushenko, P. Ivashko, Spectropolarimetry of cancer change of biotissues // *Proc. SPIE*, **7388**,73881D (2009).
27. A.P. Peresunko, A.G. Ushenko, Analysis of statistical structure of bioliquid images into cancer diagnostics // *Proc. SPIE*, **6254**, 62541R (2006).
28. A.G. Ushenko, Polarization structure of scattering laser fields // *Optical Engineerin.* **34**, (4), p.1088-1093 (1995).
29. A.G. Ushenko, Depolarization of a laser emission field as the correlation development of its polarization structure // *Proc. SPIE*, **3317**, p. 331 (1997);
30. A.G. Ushenko, Polarization contrast enhancement of images of biological tissues under the conditions of multiple scattering // *Optics and Spectroscopy*, **91**, (6) p. 937-940 (2001).
31. A.G. Ushenko, VP. Pishak, S.B. Yermolenko, O.V. Pishak, D.N Burkovets, Laser measurements of crystal optical properties of blood-formed elements // *Proc. SPIE*, **3317**, p.425-433 (1997).
32. A.G. Ushenko, Polarization correlometry of angular structure in the microrelief pattern or rough surfaces // *Optics and spectroscopy*, **92**, (2), p.227 – 229 (2002).
33. A.G. Ushenko, Laser polarimetry of polarization-phase statistical moments of the object field of optically anisotropic scattering layers // *Optics and Spectroscopy*, **91**, (2), p. 313-316 (2002).
34. A.G. Ushenko, Correlation processing and wavelet analysis of polarization images of biological tissues // *Optics and Spectroscopy*, **91**, (5), p.773-778 (2002).
35. S. H. Guminetskiy; O. G. Ushenko; I. P. Polyanskiy; A. V. Motrych; F. V. Grynchuk, The optical method for investigation of the peritonitis progressing process // *Proc. SPIE*, **7008**, p. 700827 (2008).
36. A.G. Ushenko, S.B.Yermolenko, A.G. Prydij, S.G. Guminetsky, Ion Gruia; Ovidiu Toma; K.S. Vladychenko, Statistical and fractal approaches in laser polarimetry diagnostics of the cancer prostate tissues // *Proc. SPIE*, **7008**, p. 70082C (2008).
37. O. I. Olar, A. G. Ushenko, Polarization-correlation study of biotissue multifractal structure // *Proc. SPIE*, **5067**, p. 41 - 49 (2003).
38. A.G. Ushenko, V.P. Pishak, O.V. Pishak, O.I. Olar, S.B. Yermolenko, A.G. Prydij, A. S. Arbuzov, Mueller matrices mapping of biological tissue architectonics // *Proc. SPIE*, **5477**, p. 422 - 429 (2004).
39. O.V. Angelsky, A.G. Ushenko, I.M. Vashenko, L.M. Bodnar Study of polarizing intercorrelative function of coherent images of phase-inhomogeneous layer anisotropy // *Proc. SPIE*, **5856**, p. 49 - 54 (2005).